Korean J. Chem. Eng., 39(1), 69-85 (2022)
DOI: 10.1007/s11814-021-0895-0

pISSN: 0256-1115
eISSN: 1975-7220

Numerical simulation of surface vibration effects on improvement of pool boiling heat transfer characteristics of nanofluid

Hasan Alimoradi, Sohrab Zaboli, and Mehrzad Shams†

Multiphase Flow Lab, Faculty of Mechanical Engineering, K.N. Toosi University of Technology, No. 17, Pardis St., Mollasadra Ave., Vanak Sq., Tehran 19395-1999, Iran
(*Received 11 March 2021 • Revised 30 June 2021 • Accepted 7 July 2021*)

Abstract−A numerical scheme for the effects of vibration on nanofluid pool boiling heat transfer was developed. For this purpose, a horizontal flat vibrating heated surface was considered. To model this phase-change phenomenon, the Eulerian-Eulerian approach was employed accompanied by the Rensselaer Polytechnic Institute (RPI) model to estimate the boiling heat flux on a solid surface, based on transient simulation. The k-ε turbulence model was used for simulating the Reynolds stresses appearing in the averaged Navier Stokes equation. The effects of the amplitude and frequency of vibration, nanofluid concentration along with magnitude of the heat flux on pool boiling heat transfer characteristics including heat transfer coefficient (HTC), vapor volume fraction and nanofluid velocity were studied. New analytical correlations for analyzing the heat transfer coefficient and nanofluid velocity based on the wall superheat temperature, amplitude and frequency of vibration were also developed. Results showed that applying mechanical vibration increased the boiling curve slope and the heat transfer coefficient. As a consequence, an increase of up to 30.11% and 17.5% in the heat transfer rate was achieved at lower heat fluxes for higher amplitude and frequency of oscillations, respectively.

Keywords: Pool Boiling, Mechanical Vibration, Nanofluid, Eulerian-Eulerian Approach

INTRODUCTION

Pool boiling heat transfer is a complicated and important research area in multiphase and heat transfer fields, which is widely used in various industrial applications such as heat exchangers, air conditioning systems, heat pipes, and domestic refrigerators [1,2]. The pool boiling process occurs by the formation of the vapor on the heated surface inside the stationary liquid, even though the fluid inside the pool can circulate with natural convection and bubble motions. Owing to its transient and multidimensional nature, a vast majority of the efforts have been focused on measuring and simulating the boiling process in recent decades.

Despite these complexities, industrialists have been looking for ways to improve the heat transfer process. Perhaps the most important advances in this field are related to the construction of heat transfer surfaces from hot sources to fluid with specific geometric characteristics of the surface. The construction of these surfaces is based on theories that improve the heat transfer process, such as boiling phenomena and are practically tested. But since the many parameters involved in this process are not yet fully understood, and also these parameters affect each other, it is not possible to determine the ideal level that has the maximum efficiency. There are many methods to improve two phase heat transfer which have been categorized as active and passive. Passive methods work on improving the geometry of surfaces or adding materials to the fluid. Active methods that require external energy include electric or acoustic fields or surface vibration. Access to most of the active methods outside the laboratory environment is difficult or unjustified. Passive methods include adding additives to liquids such as nanoparticles or other fluids, or improving the geometric, physical, and chemical properties of the surface. A combination of any of these techniques is termed as a compound technique. Among such techniques, applying mechanical vibration induced by external excitation on a heated surface can lead to an augmentation in the heat transfer coefficient. Note that such oscillations naturally exist in heat exchanging devices, and implementation of this technique can increase pool boiling heat transfer performance in such devices [3-8].

Numerous studies have surveyed the effects of nanofluid in boiling heat transfer coefficient. Some researchers found an increase in the heat transfer coefficient after adding nanoparticles into the base fluid [9,10]. However, others reported a decrease in heat transfer rate in nanofluids [11,12]. Two-phase flow and droplet behavior in cathode side of a single-serpentine microchannel of proton exchange membrane fuel cell have also been investigated. The results showed that as the number of passes in the channel increase, the distribution of droplet decreases, whereas distribution of film and annular flow pattern increases. Moreover, the formation of film flow in the tapered channel is more than the simple channel, and pressure fluctuation was declined in the tapered channel [13-16].

Some researchers have studied the effects of vibration on boiling phenomena experimentally. Most of them focused their research on the effects of such oscillations on boiling heat transfer coefficient enhancement or critical heat flux (CHF) improvement. Atashi et al. [17] investigated the effect of low-frequency vibrations on the

†To whom correspondence should be addressed.
E-mail: shams@kntu.ac.ir

boiling heat transfer characteristics. They found that vibrations generated new nucleation sites and turbulences, which led to the formation of smaller bubbles compared to the non-vibrating heated surface. The most notable result was that at the specific frequency of 25 Hz, the enhancement ratio of boiling heat transfer improved from 8.1% to 116.6% in the presence of low-frequency vibrations. Jeong et al. [18] investigated the effects of ultrasonic vibration on critical heat flux (CHF) for different inclination angles of the heated surface and water subcooling temperature, experimentally. Results show that the rate of enhancement in CHF increases with an increase in water subcooling temperature, while it decreases with an enhancement in inclination angle. Subsequently, Unno et al. [19] investigated the effects of vibration on the enhancement of boiling heat transfer. They attached a thin brass plate close to a heating surface. Due to the bubble growth between the heating surface and the plate, the plate was vibrating under natural vibration frequency. They found that when the natural frequency of the plate matches the frequency of the growth, the wall superheat temperature decreases by 5 K. Sathyabhama et al. [20] experimentally studied the effects of mechanical vibration of a copper flat circular surface on the pool boiling heat transfer characteristics. They investigated the effects of frequency and amplitude of vibration on the boiling heat transfer coefficient. An increase in the heat transfer coefficient was observed at low frequency and amplitude, while at higher amplitude and frequency heat transfer deteriorates. Heat transfer coefficient increases up to 26% with vibration intensity, represented by vibrational Reynolds number. In a comprehensive experimental study, Kim et al. [21] reported that employing ultrasonic vibration increases the pool boiling and natural convection heat transfer. The behavior of cavitation and thermal bubbles is observed by employing a high-speed video imaging system. Results show that the effects of ultrasonic vibration on flow behavior are dependent on the heat transfer regime and the amount of dissolved gas. They also found that the reduced thermal bubble size at departure and acoustic streaming are major factors enhancing the heat transfer rate. Alangar [22] investigated pool boiling on a flat surface induced by external excitation experimentally. Results showed that applying mechanical vibration shifts the boiling curve towards lower superheat temperatures and the slope of boiling curve decreases remarkably, when the surface is given external excitation. It was also noted that high frequency and high amplitude of oscillations led to more intensive heat transfer.

Besides the aforementioned experimental studies, some numerical surveys have been undertaken to investigate boiling phenomena. Alimoradi et al. [23] developed a numerical scheme to optimize the surface temperature and vapor volume fraction in subcooled flow boiling in a vertical channel. Pressure, mass flux, inlet subcooled temperature and heat flux were chosen as variables of optimization. They concluded that the numerical simulation results were in good agreement with the experimental results. Shoghl et al. [24] numerically investigated bubble dynamics in nanofluid pool boiling using sodium dodecyl sulfate (SDS) solution with various nanoparticles. They experimentally investigated microscale parameters, including contact angle and shape of bubbles and verified them using CFD simulation. They found that the growth time of bubbles changes by the existence of porous layers and surfactant solution. Number of bubbles also declined by CuO and Al_2O_3 nanofluid boiling. Valizadeh et al. [25] numerically investigated water-based nanofluid subcooled flow boiling by three-phase Euler-Euler, Euler-Lagrange approach. In this new scheme, three separate phases, including water, vapor, and nanoparticles, were considered. Results show that the addition of 0.0935% volume fraction of nanoparticles in pure liquid boiling flow enhances the vapor volume fraction at the outlet almost by 40.7%. Kamel et al. [26] simulated pool boiling of nanofluid using Eulerian-Eulerian approach. The surface modification during silica nanofluid pool boiling simulation represented by surface roughness and wettability was taken into consideration in the simulation. This was done by applying new correlations for bubble departure diameter and nucleation site density. The results found that considering the surface modification of nucleate pool boiling parameters would give more mechanistic sights compared to the classical model utilized for predicting pure liquid boiling heat transfer.

Numerical Studies on nanofluid pool boiling accompanied by the effects of surface vibration are very limited. The effects of vertical vibration on pool boiling heat transfer of an array of tubes were numerically investigated by Noori et al. [27] recently. Water at atmospheric pressure conditions was chosen as the boiling liquid, and boiling occurred on the surface of heated tubes. Their results showed that applying mechanical vibration enhances the heat transfer coefficient (HTC) up to 90%. It was also reported that increasing effect of the vibration was so dominant at low heat fluxes.

Previous numerical investigations were used to examine the effects of horizontal or vertical vibration on heat transfer performance of an array of tubes [28-30]. However, to the author's best knowledge, no attempt has been made so far to examine the effects of vibration on nanofluid pool boiling heat transfer on a flat horizontal surface. Hence, we numerically investigated nanofluid pool boiling on a heated surface vibrating under specific circumstances. Silica nanofluid at saturation temperature and atmospheric pressure conditions was chosen and a comprehensive study on the effects of amplitude and frequency of oscillations on the pool boiling heat transfer characteristics of silica nanofluid was undertaken.

MATHEMATICAL FORMULATION

1. Assumptions

The Euler-Euler formulation is based on the assumption of interpenetrating continua. A separate set of mass, momentum and energy conservation equations is solved for each phase. Interphase transfer terms have to be modeled to account for the interaction of the phases. The Eulerian two-phase model was used to simulate the pool boiling of the nanofluid. Due to the dilute concentration of nanoparticles in the base fluid, it was assumed that nanofluid surface tension is the same as pure water, and nanofluid behaves as a homogenous fluid. As a consequence, it is rational to consider the nanofluid as a single-phase liquid. It was also reported by [31-34] that the thermal properties of dispersed phase were not affected by deposited nanoparticles stemming from low vapor density. For this model, the nanofluid and vapor were considered the continuous flow and dispersed flow, respectively. The effective thermophysical properties of nanofluid are as follows:

Density, introduced by [34]:

$$\rho_{eff}=\varphi\rho_p+(1-\varphi)\rho_l \tag{1}$$

Heat capacity, introduced by [34]:

$$C_{p,\,eff}=\frac{\varphi\rho_p C_{p,\,p}+(1-\varphi)\rho_l C_{p,\,l}}{\rho_{eff}} \tag{2}$$

Thermal conductivity, used by [35]:

$$k_{eff}=\left[\frac{k_p+(n-1)k_l-\varphi(n-1)(k_l-k_p)}{k_p+(n-1)k_l+\varphi(k_l-k_p)}\right]k_l \tag{3}$$

Viscosity, used by [36]:

$$\mu_{eff}=\frac{\mu_l}{(1-\varphi)^{-2.3}} \tag{4}$$

2. Governing Equation

The pool boiling equations in Euler-Euler approach are as follows. The nanofluid is considered as continuous phase and vapor is the dispersed phase. Eq. (5) and Eq. (6) show the continuity equations for the liquid and vapor phase [23].

$$\frac{\partial(\rho_l\alpha_l)}{\partial t}+\nabla\cdot(\rho_l\alpha_l\mathbf{u}_l)=\Gamma_{lg} \tag{5}$$

$$\frac{\partial(\rho_g\alpha_g f_i)}{\partial t}+\nabla\cdot(\rho_g\alpha_g\mathbf{u}_g)=S_i-f_i\Gamma_{lg} \tag{6}$$

Eq. (7) and Eq. (8) show the momentum equations for the liquid and vapor phases [23].

$$\begin{aligned}&\frac{\partial\rho_l\alpha_l\mathbf{u}_l}{\partial t}+\nabla\cdot(\rho_l\alpha_l\mathbf{u}_l\mathbf{u}_l)\\&=-\alpha_l\nabla P+\alpha_l\rho_l\mathbf{g}+\nabla[\alpha_l\mu_l^e(\nabla\mathbf{u}_l+(\nabla\mathbf{u}_l)^T)]+(\Gamma_{lg}\mathbf{u}_g-\Gamma_{gl}\mathbf{u}_l)+F_{lg}\end{aligned} \tag{7}$$

$$\begin{aligned}&\frac{\partial\rho_g\alpha_g\mathbf{u}_g}{\partial t}+\nabla\cdot(\rho_g\alpha_g\mathbf{u}_g\mathbf{u}_g)\\&=-\alpha_g\nabla P+\alpha_g\rho_g\mathbf{g}+\nabla[\alpha_g\mu_g^e(\nabla\mathbf{u}_g+(\nabla\mathbf{u}_g)^T)]+(\Gamma_{gl}\mathbf{u}_g-\Gamma_{gl}\mathbf{u}_g)+F_{gl}\end{aligned} \tag{8}$$

The energy equation for the liquid and vapor phases is shown in Eq. (9) and Eq. (10), respectively [23].

$$\frac{\partial\rho_l\alpha_l H_l}{\partial t}+\nabla\cdot(\rho_l\alpha_l\mathbf{u}_l H_l)=\nabla[\alpha_l k_l^e(\nabla T_l)]+(\Gamma_{gl}H_l-\Gamma_{lg}H_g) \tag{9}$$

$$\frac{\partial\rho_g\alpha_g H_g}{\partial t}+\nabla\cdot(\rho_g\alpha_g\mathbf{u}_g H_g)=\nabla[\alpha_g k_g^e(\nabla T_g)]+(\Gamma_{lg}H_l-\Gamma_{gl}H_g) \tag{10}$$

In all aforementioned equations ρ_l, ρ_g, α_l, α_g, $\mathbf{u}_l$ and $\mathbf{u}_g$ are liquid density, vapor density, liquid volume fraction, vapor volume fraction, liquid velocity and vapor velocity, respectively. μ_l is the liquid dynamic viscosity in Eq. (7) and μ_g is the vapor dynamic viscosity in Eq. (8). H_l, H_g, k_l and k_g are liquid enthalpy, vapor enthalpy, liquid thermal conductivity, and vapor thermal conductivity, respectively. It should be taken into consideration that the variable **u** appearing in the convection terms of Eq. (5) to Eq. (10) is defined as the absolute velocity, which is calculated from the difference between the bulk fluid and mesh velocities ($\mathbf{u}-\hat{\mathbf{u}}$). The term $\hat{\mathbf{u}}$ is the grid velocity. This method was utilized successfully by previous researchers [27-29].

F_{lg} is the applied force by vapor phase on the liquid phase. The applied force by the liquid phase on the vapor phase is shown by F_{gl} and the correlation between these forces is $F_{lg}=-F_{gl}$.

In the simulation, Γ_{lg} is the mass transfer rate between two phases in the subcooled liquid that is due to distillation. This parameter is calculated from below [23]:

$$\Gamma_{lg}=\frac{h a_{if} T_{sub}}{h_{fg}} \tag{11}$$

where, h is the heat transfer coefficient between two phases in Eq. (11). Γ_{gl} is the vapor generation rate that is considered as the overall mass of the separated bubbles from the wall surface under the heat flux. Γ_{gl} is calculated by [23]:

$$\Gamma_{gl}=\frac{Q_e}{h_{fg}} \tag{12}$$

The k-ε turbulence model was used for simulating the Reynolds stresses in the averaged Navier Stokes equation. The Ishii-Zuber [37] model was adopted to measure the drag forces between two phases.

$$C_D=\mathrm{Min}(C_{D,vis},\,C_{D,dis}) \tag{13}$$

where; C_D is the drag coefficient and is calculated by choosing the minimum value between $C_{D,vis}$ and $C_{D,dis}$ which are defined as the viscous regime and the distorted regime coefficient, respectively.

$$C_{D,\,vis}=\frac{24}{Re}(1+0.15Re^{0.75}) \tag{14}$$

$$C_{D,\,dis}=\frac{2}{3}\frac{d_{bubble}}{\sqrt{\dfrac{\sigma}{g(\rho_l-\rho_g)}}} \tag{15}$$

where; Re is the relative Reynolds number as shown in Eq. (14), σ is the surface tension, and g is the gravitational acceleration and d_{bubble} is the bubble diameter.

$$Re=\frac{\rho_l|\mathbf{u}_g-\mathbf{u}_l|d_g}{\mu_l} \tag{16}$$

The heat transfer coefficient in liquid phase was calculated by Ranz and Marshall model [38] as follows:

$$Nu_g=2.0+0.6Pr_l^{0.333}\,Re_g^{0.5} \tag{17}$$

where; Re_g is the relative Reynolds number based on the diameter of the dispersed phase (bubble diameter), and relative velocity $|\mathbf{u}_g-\mathbf{u}_l|$, and Pr_l is the Prandtl number of the continuous phase (nanofluid) as follows:

$$Pr=\frac{C_{p,\,l}\mu_l}{k_l} \tag{18}$$

The Lopez de Bertodano [39] model was selected for calculating the turbulent dispersion force in this simulation as follows:

$$\vec{F}_{td,\,l}=-\vec{F}_{td,\,g}=C_{TD}\rho_l K_l\nabla\varphi_g \tag{19}$$

The heat transfer behavior of the heated surface during the pool boiling phenomena was mainly determined by the popular heat flux partitioning model, which has been labeled as the 'RPI model' [40,41]. According to this classic model, the total heat flux Q_{total} from the heated surface in the boiling process can be divided into three types: heat transferred to the liquid phase outside the zone of

influence of the bubbles by convection Q_c, the latent heat of evaporation to form the bubbles Q_e, and the quenching heat flux Q_{tc}, that is the amount of transient energy which is related to agitated liquid layer from the upper part of the heated surface by departed bubble [31-33,42].

The turbulent convection heat flux is calculated by Eqs. (20)-(22) [43].

$$Q_c = A_{1f}\frac{\rho_L C_{pl}\mathbf{u}_l}{T^+_{y^+(L)}}(T_W - T_l) \tag{20}$$

$$A_{1f} = 1 - A_{tc} \tag{21}$$

$$A_{tc} = \min\left(\pi\frac{(a d_W)^2}{4}, 1\right) \tag{22}$$

where, $T^+_{y^+(L)}$ is the non-dimensional temperature and a is the bubble influence factor that is equal to two. The heat flux due to evaporation is calculated by Eq. (23). In this correlation $\dot{m}_W$ is the mass flux of bubbles formed in the active nucleation sites. The mass flux is calculated by Eq. (24) [43]:

$$Q_e = \dot{m}_W h_{fg} \tag{23}$$

$$\dot{m}_W = \rho_g \frac{2}{3}\frac{d_w}{a^2} A_{tc} N_a f \tag{24}$$

The heat transfer mechanism for a stagnant or near wall bubble is conduction heat transfer. This heat transfer between fluid and wall is called transient heat transfer, which is expressed by [43]:

$$Q_{tc} = \left(\frac{2}{\sqrt{\pi}}\sqrt{k_l \rho_l C_{pl} f}\right) A_{tc}(T_w - T_l) \tag{25}$$

In the above equations, N_a is the active nucleation site density and f is bubble departure frequency. The active nucleation site density is defined based on the superheat temperature. A new correlation based on the experimental results of nanofluid nucleation site density is estimated by Li et al. [33] for silica nanofluid nucleation site density to tackle the nanoparticle wettability characteristics in boiling phenomena. Thus, this correlation is adopted in the present study.

$$N_a[m^{-2}] = 1.206\times 10^4 (1-\cos\theta)\Delta T_{sup}^{2.06} \tag{26}$$

For the bubble departure diameter the following correlation is applied by Tolubinsky and Kostanchuk [44].

$$d_w = \min\left(0.6[mm]\exp\left(\frac{-\Delta T_{sub,\,Lw}}{45K}\right), 1.4[mm]\right) \tag{27}$$

This model is derived for the high-pressure water boiling experimental data with the upper limit for the bubble departure diameter d_w=1.4 mm.

In the present simulation, a polynomial correlation defined by Kamel et al. [26] was utilized to propose the bubble departure diameter of silica nanofluid pool boiling. This correlation is adopted from the experimental results of Gerardi et al. [45].

$$d_w = -1.91\times 10^{-3} + 4.21125\times 10^{-4}\Delta T_{sup} - 1.70945\times 10^{-5}\Delta T_{sup}^2 + 2.03938\times 10^{-7}\Delta T_{sup}^3 \tag{28}$$

A simple estimation of the bubble departure frequency as the terminal rise velocity over the bubble departure diameter is adopted [46].

$$f = \sqrt{\frac{4\mathbf{g}(\rho_l - \rho_g)}{3 d_w \rho_l}} \tag{29}$$

The time between bubble departure and appearing of the next bubble in the same nucleation site is the waiting time. In the present work, the correlation by Kurul and Podowski [40] is used to measure the waiting time.

$$t_w = \frac{0.8}{f} \tag{30}$$

3. Boundary Conditions

In the present work, the associated boundary conditions are as follows:

1. Heated surface is maintained at constant heat flux.

$$q'' = -k_w\frac{\partial T}{\partial x} = \text{const}$$

2. At adiabatic walls heat flux is set to zero.

$$q'' = -k_w\frac{\partial T}{\partial x} = 0$$

3. Top of the boiling chamber is assumed to be at atmospheric pressure condition.

$$P = P_{atm}$$

4. Problem Description

A rectangular domain in 2-Dimension was considered as the pool boiling chamber [47] to investigate the effects of mechanical vibration on nanofluid pool boiling heat transfer. The dimensions of the corresponding boiling chamber were (300×150 mm), with the heated surface with 40 mm located in the middle of the chamber. The simulation was done using silica nanofluid at saturation temperature and atmospheric pressure conditions. Consequently, boiling takes place on the center of the bottom chamber. Furthermore, vertical vibration induced by external excitation is applied on the heated surface using a periodic displacement of $Y = Y_{wall}\sin(2\pi f_{vib} t)$, where t is time, Y_{wall} is the amplitude of the vibration, and f_{vib} is its frequency. Fig. 1 shows the schematic of the considered physical domain for the present study.

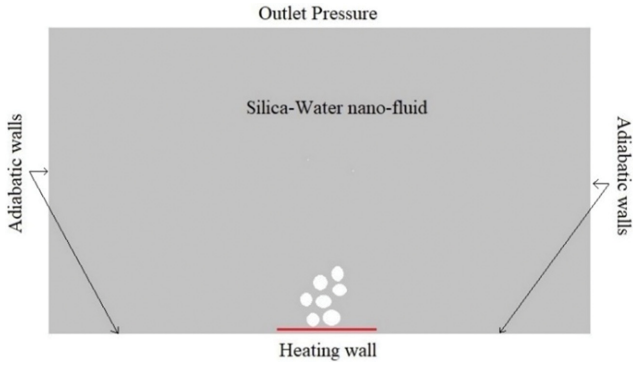

Fig. 1. Geometry description of pool boiling model.

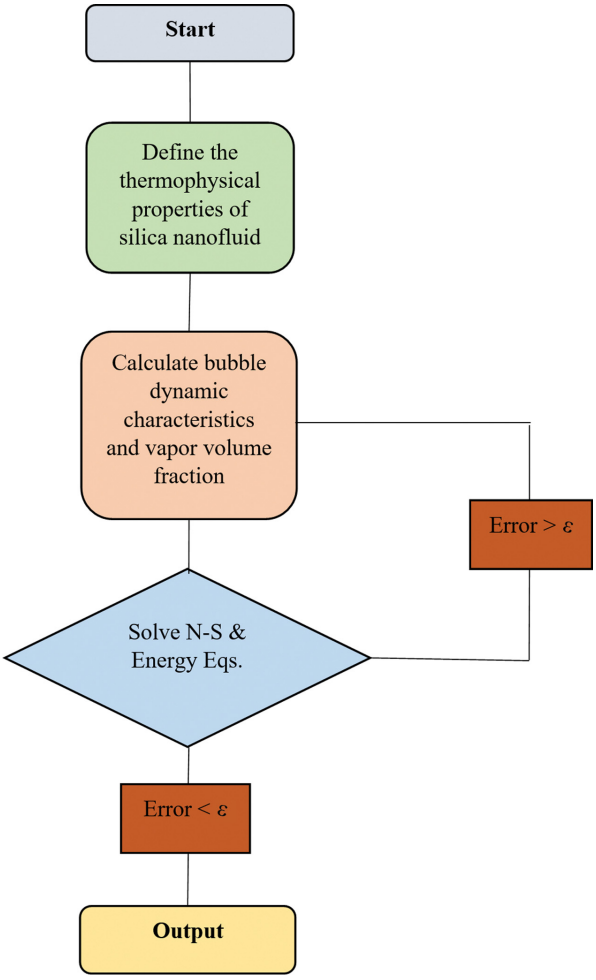

Fig. 2. Flowchart of the proposed algorithm for the present study.

NUMERICAL METHOD

1. Flow Solver

The governing equations of pool boiling presented in Eq. (1) are numerically solved using commercial CFD code. A second-order spatial and temporal discretization was adopted, and convective heat fluxes were approximated by a high-resolution scheme. Transient simulations were conducted using a timestep of 10^{-3} s, and the global convergence criterion was set at 10^{-4}.

Fig. 2 illustrates the general algorithm for solving Eq. (5) to Eq. (10). This process begins with an initial assumption. Having calculated the thermophysical properties of silica nanofluid using Eq. (1) to Eq. (4), the numerical procedure then computes the bubble dynamic characteristics such as nucleation site density, bubble departure diameter and bubble detachment frequency. After that, the Navier-Stokes and energy equations are solved. Finally, it compares the error with the convergence criterion to return to the previous steps or end.

In addition, the following assumptions are considered for the simulations:

1. The flow field is two dimensional and transient.
2. The properties of each phase are assumed to be constant under the specified operating conditions.
3. The interface temperature is assumed to be at the saturation temperature.
4. A no-slip condition is considered for all walls within the computational domain.
5. At the beginning of the simulation, the flow field is quiescent at a temperature of 373.15 K.
6. The upper part of the pool is opened to attain saturation pressure.

2. Grid Independency and Validation

The experimental study of Gerardi et al. [45] was used to investigate the accuracy of the numerical simulation. The considered geometry is mentioned in previous sections. Fig. 3(a) shows the applied heat flux versus the averaged superheat temperature of the heated surface for four different grids. Furthermore, Fig. 3(b) shows the averaged vapor volume fraction along the vertical distance for four different grids. The averaged vapor volume fraction is increased sharply near the heated surface, which indicates that the boiling starting point is well predicted by the simulation. It is observed that there is a slight difference between the cases. Hence, the averaged superheat temperature of the heated surface is independent of element grid size for element size of 0.9 mm. Grid structure of the whole computational domain is shown in Fig. 4.

Fig. 5(a) shows the bubble departure diameter versus superheat temperature for the present model compared to the experimental data of Gerardi et al. [45] and previous study [26]. Fig. 5(a) indicates that Eq. (28) predicts bubble departure diameter of silica nanofluid better than Eq. (27). Moreover, a comparison was undertaken between the present study and available correlations from the literature for nanofluid nucleation site density, as shown in Fig. 5(b). The difference between the experimental and simulation values of nucleation site density at high heat flux region, which was also reported in the experimental work of Li et al. [33], is that as the heat flux increases, bubbles which are formed on the heated surface are integrated and this leads to bubble coalescence. This factor decreases the formation of bubbles in the experimental procedure. It can be seen that bubble dynamics characteristics are predicted successfully with Eq. (26) and Eq. (28). As a consequence, these correlations were utilized to validate the silica nanofluid boiling curve in the present study. The averaged heated surface temperature and heat transfer coefficient were compared with the experimental data [45] and previous numerical study [26] for silica nanofluid (0.01% vol) and are depicted in Fig. 6(a) and Fig. 6(b). Numerical results are in very good agreement with experimental data and previous numerical simulation. Fig. 6(c) compares the results obtained from the present study for silica nanofluid (0.01% vol) with the experimental data of Gerardi et al. [45] for water. It can be seen that compared to water HTC decreases when using nanofluid as continuous phase. The deposition of nanoparticles on the heated surface and its effect on pool boiling heat transfer is heavily dependent on the material, size, and concentration of nanoparticles as well as the hydrophobic or hydrophilic behavior of the surface during the formation of the bubbles on the heated wall. Moreover, nanoparticle addition to the base fluid (water) modifies surface characteristics and either increases or decreases HTC. Deposition of these nanoparticles builds up the porous micro-layer,

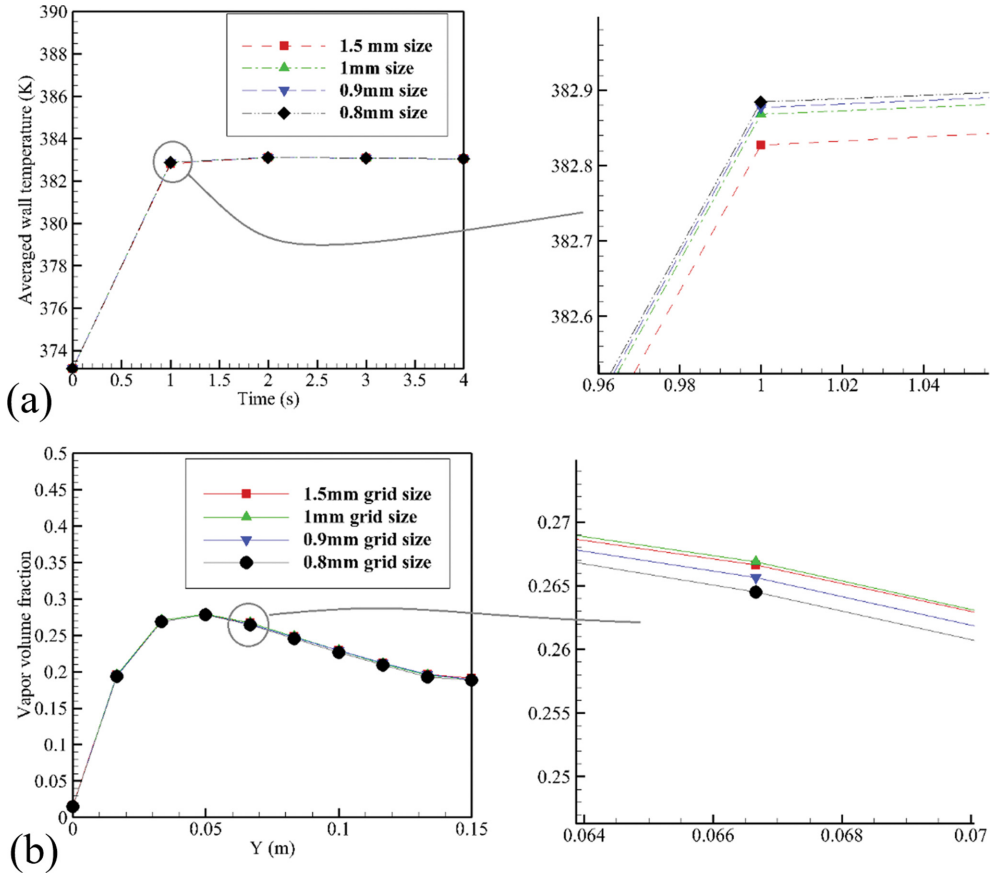

Fig. 3. (a) Averaged heated surface temperature and (b) averaged vapor volume fraction along the vertical distance at t=4 s.

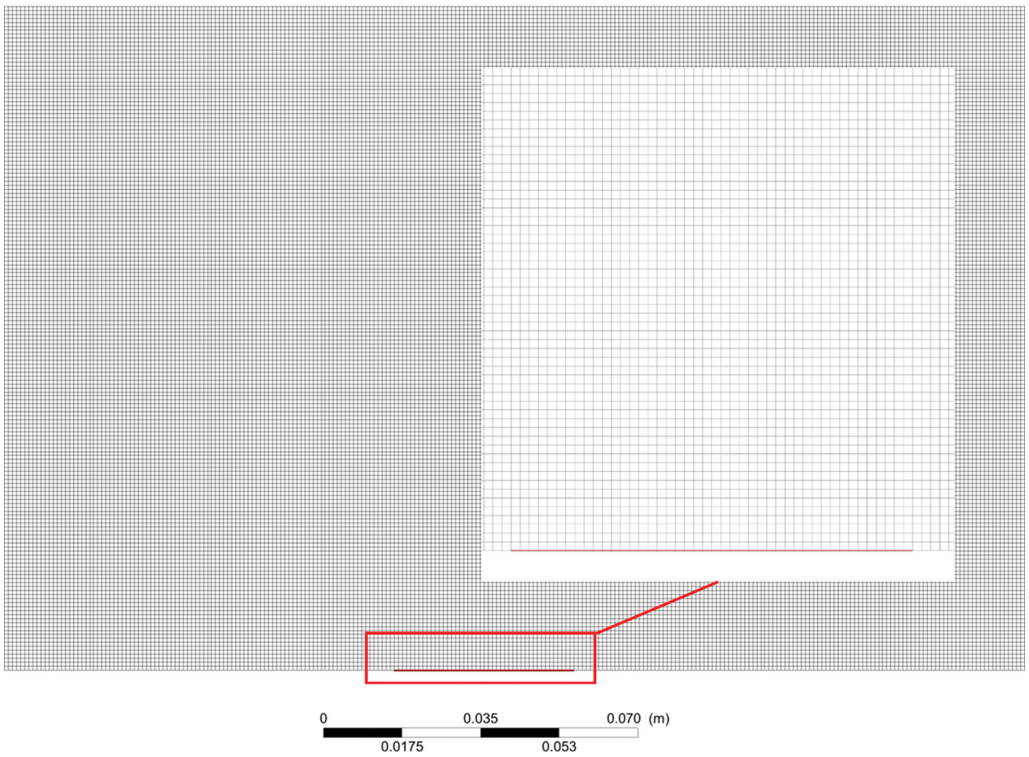

Fig. 4. Grid structure view.

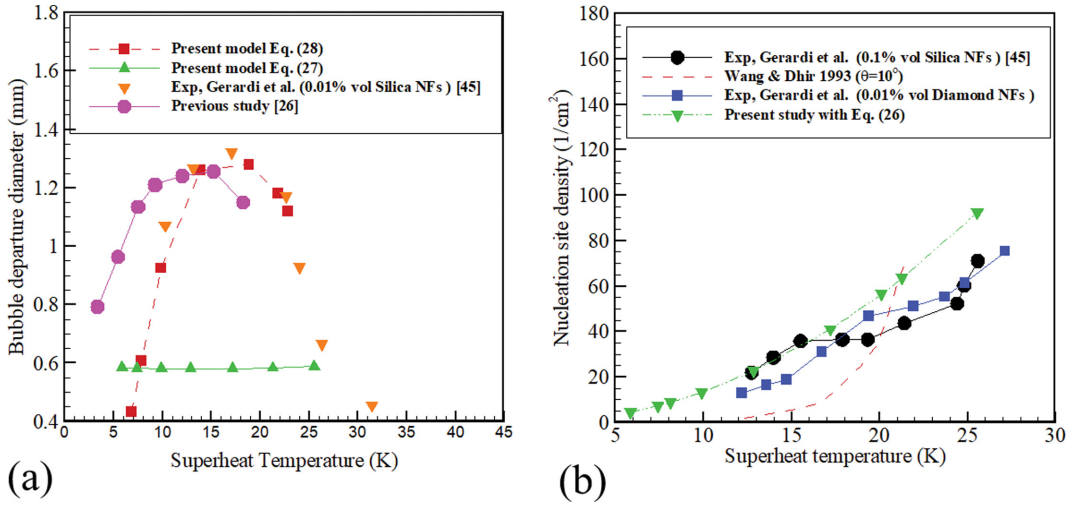

Fig. 5. Nanofluid bubble dynamic characteristics (a) bubble departure diameter against superheat temperature in the present model compared to the experimental data of Gerardi et al. [45] and (b) nucleation site density against superheat temperature for the present model and available correlations from the literature.

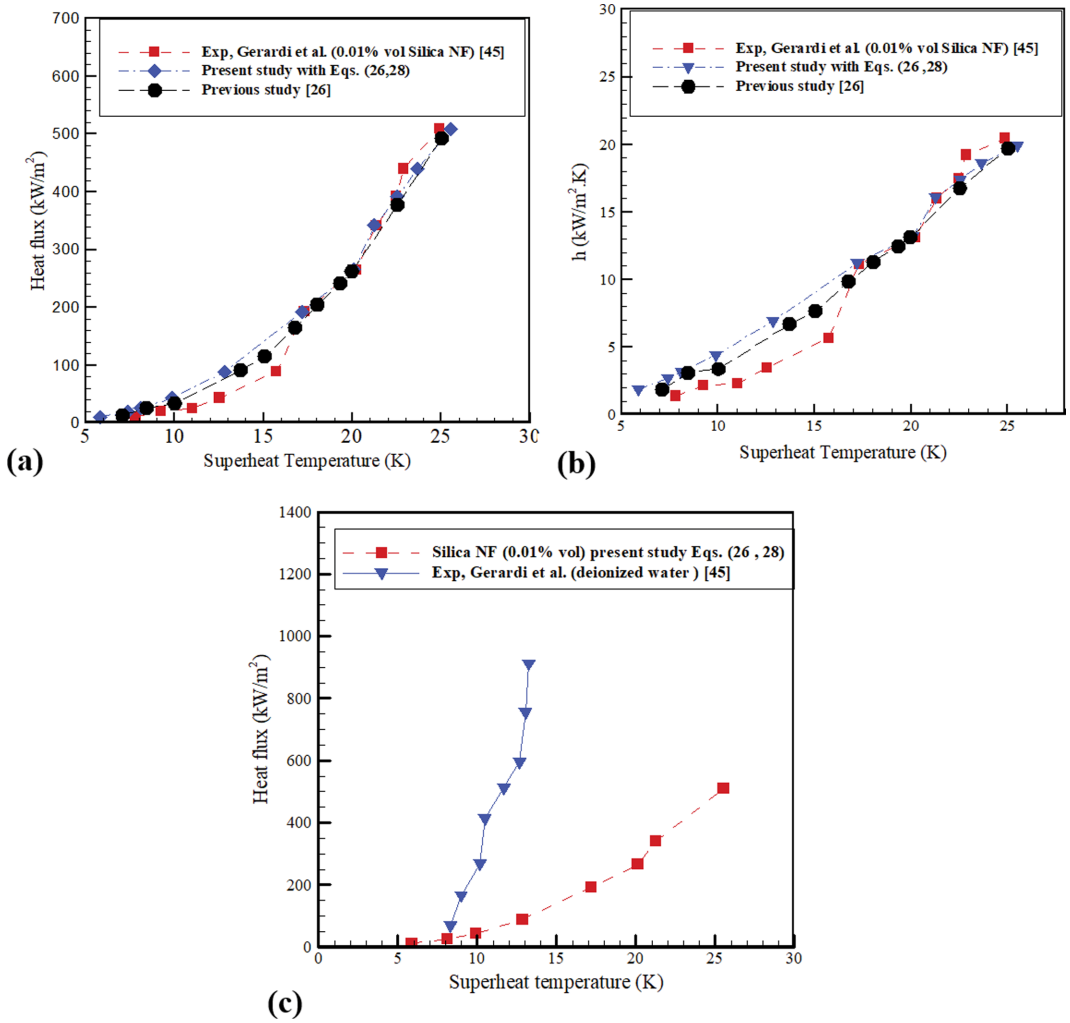

Fig. 6. Silica nanofluid (0.01% vol) pool boiling validation between the present model, experimental data of Gerardi et al. [45] and previous study [26] (a) boiling curve, (b) heat transfer coefficient, and (c) comparison between present model and experimental data of Gerardi et al. [45] for water.

primarily created due to micro-layer evaporation process, on the heated surface and delays the rate of heat transfer from the surface to the liquid. This was also reported by Kamel et al. [26] and Gerardi et al [45]. Likewise, in this study the effect of sedimentation on contact angle was considered using Eq. (26) to predict nucleation site density, and Eq. (28) to estimate bubble departure diameter of nanofluid. As the nanofluid concentration increases, contact angle rises and nucleation site density proposed by Eq. (26) improves. This improvement in the nucleation site density leads to a decrease in bubble departure diameter. The reduction of bubble departure diameter causes faster detachment of bubbles from the heated surface, which finally decreases wall superheat temperature and enhances HTC.

RESULTS AND DISCUSSION

In this section, the effects of important parameters, such as the impact of amplitude and frequency of oscillations, heat flux applied to the heated surface, and nanofluid concentration on parameters such as vapor volume fraction, nanofluid velocity and boiling curve, are investigated.

1. The Effects of Vibration Amplitude

Fig. 7(a) displays the effect of vibration amplitude on the boiling curve of silica nanofluid (0.01%vol). Fig. 7(b) exhibits the effect of vibration amplitude on the heat transfer coefficient of silica nanofluid (0.01%vol). Fig. 7(a) and 7(b) show that as the amplitude of vibration increases, boiling curve of silica nanofluid shifts towards lower superheat temperature and it causes an increase in heat transfer coefficient. Physically, this is due to the fact that by applying mechanical vibration on the surface of the heater, the bubbles formed on the surface are separated faster and the bubble detachment frequency rises. Increasing the bubble detachment frequency decreases the bubble departure diameter, which is a positive factor in the heat transfer process. As the bubbles detached from the surface become smaller, the process of bubble coalescence lessens, which is an effective agent in delaying the CHF. Heat transfer improvement is much higher in the lower heat fluxes compared to the higher heat fluxes, and results are close to the non-vibrating surface in the high heat flux region. This trend is similar to the works of Alangar [22] and Noori et al. [27] on a single and array of heated tubes, respectively. The relative percentage of increment of the heat transfer rate is up to 30.11% for q=10.91 kW/m^2 and 3.94% for q=265.5 kW/m^2 compared to the non-vibrating surface, when Y_{wall}= 3 mm and f_{vib}=10 Hz. As a result, the amplitude of vibration plays an important role in the pool boiling heat transfer enhancement at the lower heat fluxes. Fig. 7(c) shows the effect of vibration ampli-

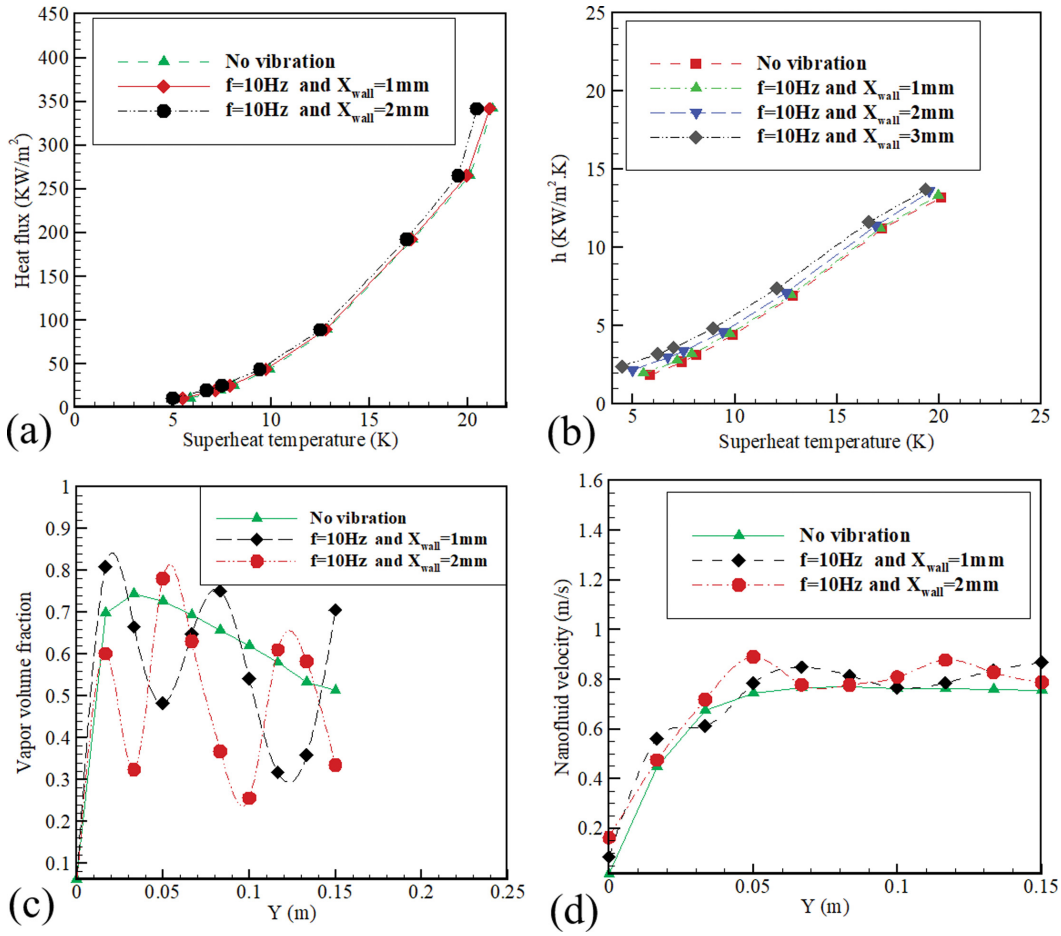

Fig. 7. Effect of vibration amplitude on silica nanofluid (0.01% vol) pool boiling heat transfer characteristics at t=4 s (a) boiling curve, (b) heat transfer coefficient, (c) vapor volume fraction along the vertical distance, and (d) nanofluid velocity along the vertical distance.

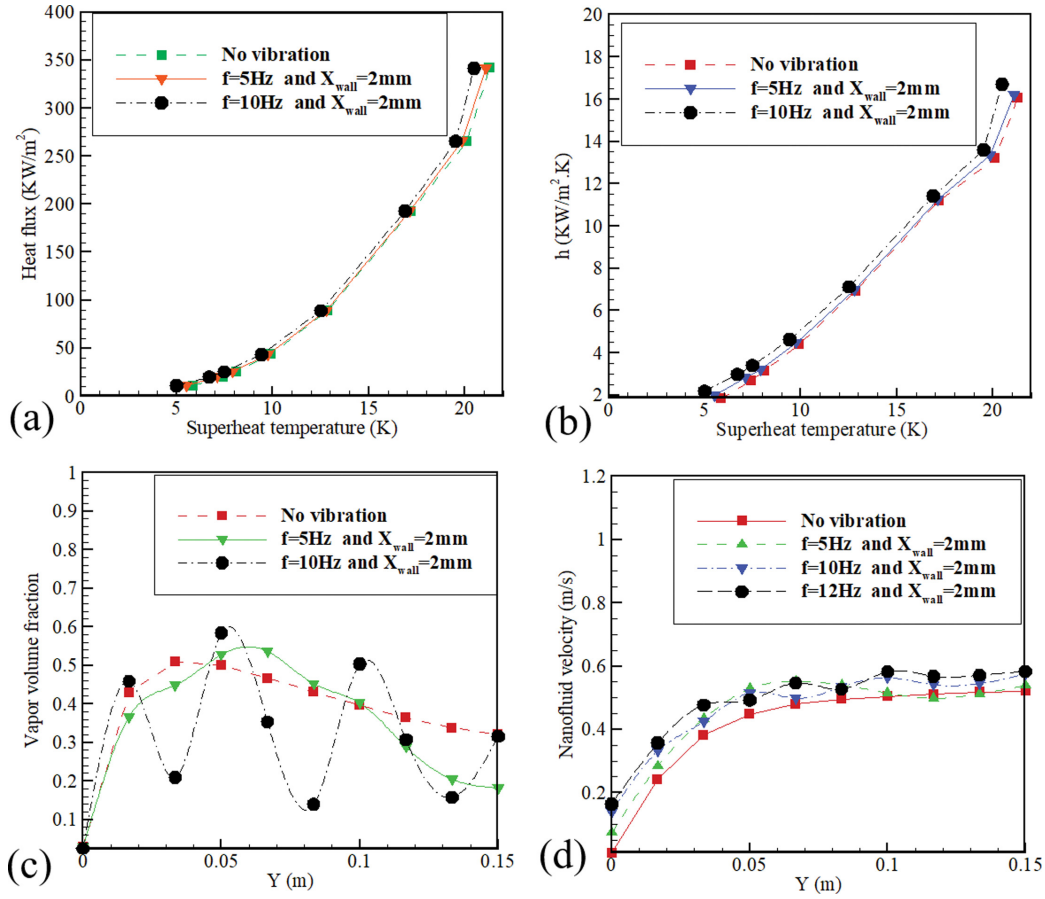

Fig. 8. Effect of vibration frequency on silica nanofluid (0.01% vol) pool boiling heat transfer characteristics at t=4 s (a) boiling curve, (b) heat transfer coefficient, (c) vapor volume fraction along the vertical distance, and (d) nanofluid velocity along the vertical distance.

tude on the vapor volume fraction along the vertical distance at t=4 s for silica nanofluid (0.01% vol) when q=192.7 kW/m^2. Fig. 7(d) shows the effect of vibration amplitude on the nanofluid velocity along the vertical distance at t=4 s for silica nanofluid (0.01% vol) when q=192.7 kW/m^2. Results show that an increase in the amplitude of vibration can bring about reduction in the averaged vapor volume fraction and an increment in nanofluid velocity. As the amplitude of vibration increases, periodic displacement also enhances. This can give rise to growth in nanofluid velocity.

2. The Effect of Vibration Frequency

Fig. 8(a) displays the effect of vibration frequency on the boiling curve of silica nanofluid (0.01%vol). Fig. 8(b) exhibits the effect of vibration frequency on the heat transfer coefficient of silica nanofluid (0.01%vol). It can be observed that as the frequency of vibration increases, superheat temperature decreases and heat transfer coefficient enhances. Again, the major reason for this pattern is that increasing the frequency of vibration causes faster separation of bubbles from the heated surface. Increasing the bubble detachment frequency decreases the bubble departure diameter. As the size of bubbles detached from the surface becomes smaller, the process of bubble coalescence becomes slower and improves heat transfer coefficient. In low heat fluxes, the percentage of heat transfer development is a bit higher than high heat fluxes, and results are close to non-vibrating surface in high heat flux region. This was also reported in previous works [22,27]. The relative percentage of increment of heat transfer rate is up to 17.5% for q=10.91 kW/m^2 and 3.9% for q=341.8 kW/m^2 compared to non-vibrating surface, when Y_{wall}=2 mm and f_{vib}=10 Hz. As a result, the frequency of vibration is a significant agent in pool boiling heat transfer enhancement at lower heat fluxes.

Fig. 8(c) shows the effect of vibration frequency on the vapor volume fraction along the vertical distance at t=4 s for silica nanofluid (0.01% vol) when q=89.09 kW/m^2. Fig. 8(d) shows the effect of vibration frequency on the nanofluid velocity along the vertical distance at t=4 s for silica nanofluid (0.01% vol) when q=89.09 kW/m^2. It demonstrates that an increase in the frequency of vibration can bring about reduction in averaged vapor volume fraction and an increment in nanofluid velocity. As the frequency of vibration increases, angular velocity also enhances, that brings about enhancement in grid displacement. This can lead to growth in nanofluid velocity. A comparison between the effects of amplitude and frequency of vibration shows that the amplitude of oscillation affects the cooling performance more than the frequency of vibration. However, the frequency of vibration decreases the vapor volume fraction less than the amplitude of vibration.

3. The Effects of Heat Flux

Fig. 9 shows the contour of vapor volume fraction along the vertical distance in four different times, for silica nanofluid (0.01%

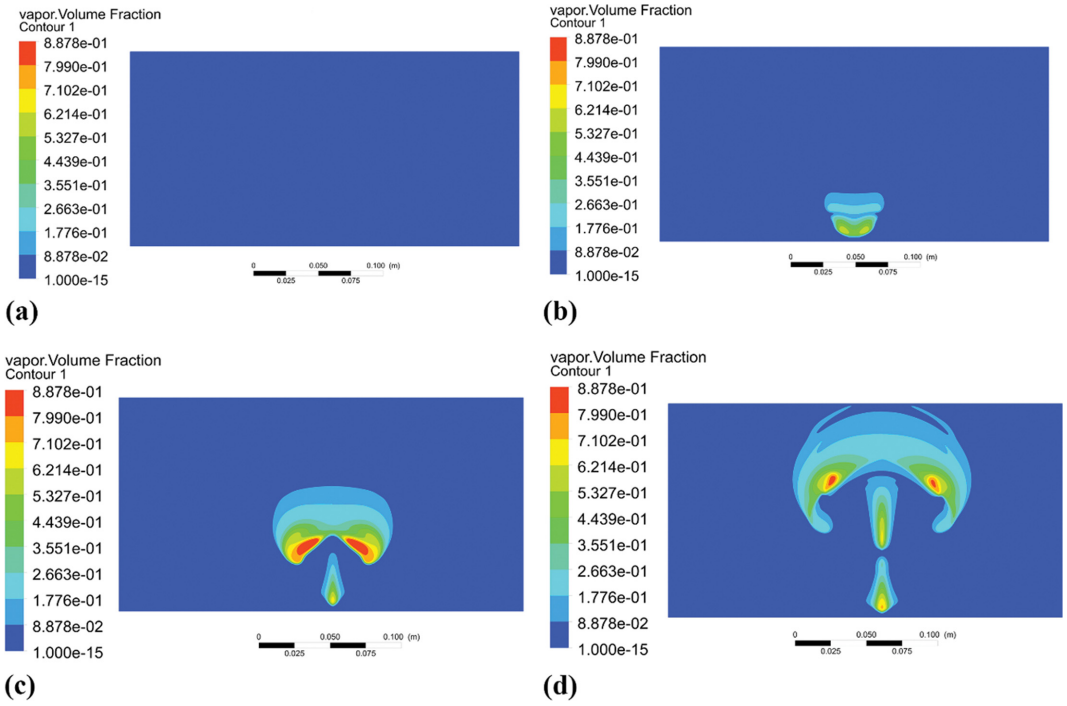

Fig. 9. Effect of mechanical vibration on vapor volume fraction for (a) t=0.1 s, (b) t=0.3 s, (c) t=0.5 s, and (d) t=0.7 s (q=192.7 kW/m^2, f_{vib}= 10 Hz, and Y_{wall}=2 mm).

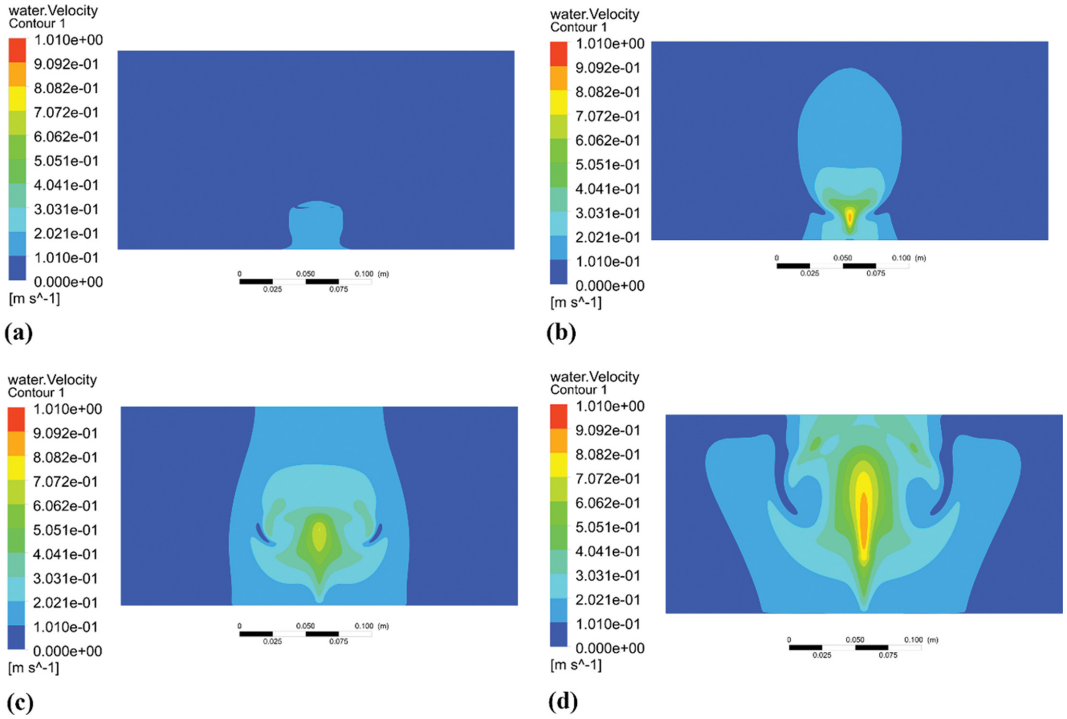

Fig. 10. Effect of mechanical vibration on nanofluid velocity for (a) t=0.2 s, (b) t=0.4 s, (c) t=0.6 s, and (d) t=0.8 s (q=192.7 kW/m^2, f_{vib}= 10 Hz, and Y_{wall}=2 mm).

vol) when q=192.7 kW/m^2, while the heated surface is at f_{vib}= 10 Hz and Y_{wall}=2 mm at t=0.3 s the bubble starts to form on the heated wall and as the time elapses the volume of the vapor bubbles becomes large, and vapor volume fraction's mushroom shape continues to grow over time. In comparison to the non-vibrating surface, the vapor volume fraction grows fragmentarily, which indicates that surface oscillation is predicted successfully in this model. Fig. 10 displays the contour of nanofluid velocity along the

vertical distance in four different times for q=192.7 kW/m^2, while the heated surface is at f_{vib}=10 Hz and Y_{wall}=2 mm. Fig. 10 shows that the nanofluid velocity enhances at the top of the heated surface by time. This is due to the enhancement of thermal momentum at this region which causes more agitation and increases the nanofluid velocity. However, the nanofluid velocity decreases and tends to zero by approaching to the adiabatic walls at all times, which is mainly because of thermal momentum reduction.

Fig. 11 exhibits the streamlines in four different times, for silica nanofluid (0.01% vol) when q=192.7 kW/m^2, while the heated surface is at f_{vib}=10 Hz and Y_{wall}=2 mm. Vorticities are formed under the mushroom cap during the pool boiling heat transfer which show the agitation mechanism in this phenomenon. These vorticities circulate water under the bubbles and replace the fresh water with that one in the vicinity of heated wall and operate as a small pump. As the size of the bubbles increases, this effect exacerbates [48]. Parallels can be drawn between this model and the non-vibrating surface in such a way that oscillations can damp the eddies formed in the heated surface which can consequently improve the pool boiling heat transfer performance. Results obtained in Figs. 9 to 11 are relatively well consistent with previous work of Aminfar et al. [48] in terms of predicting the mushroom-shape of vapor volume fraction at different times as well as vorticities formed under mushroom cap for non-vibrating heated surface.

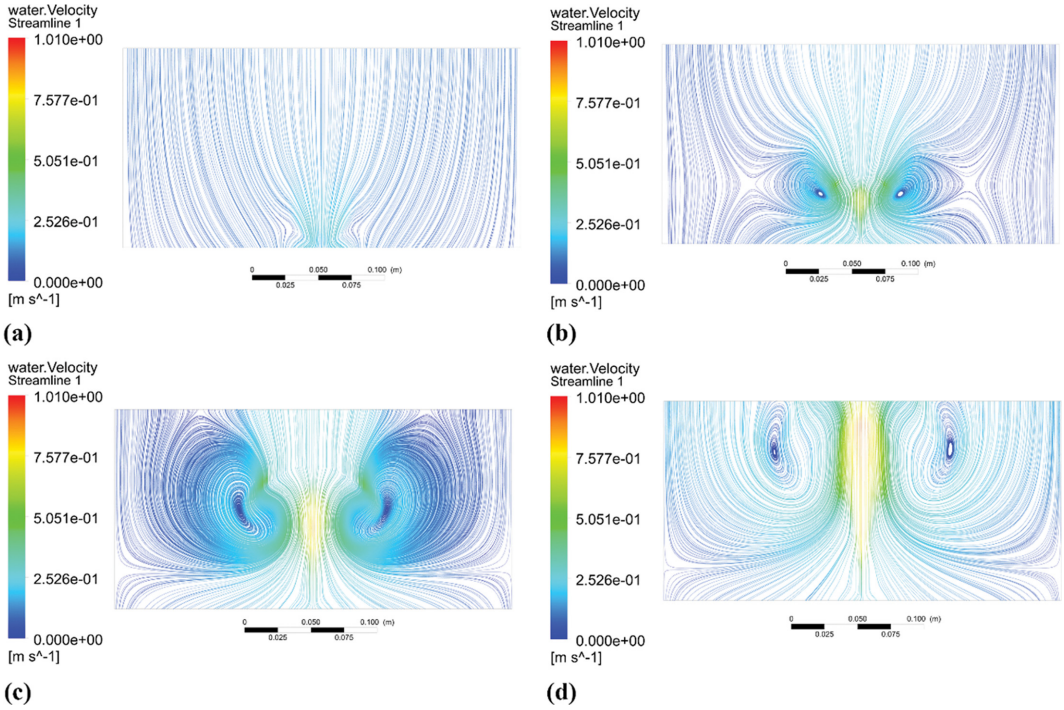

Fig. 11. Effect of mechanical vibration on streamlines for (a) t=0.3 s, (b) t=0.5 s, (c) t=0.7 s, and (d) t=0.9 s (q=192.7 kW/m^2, f_{vib}=10 Hz, and Y_{wall}=2 mm).

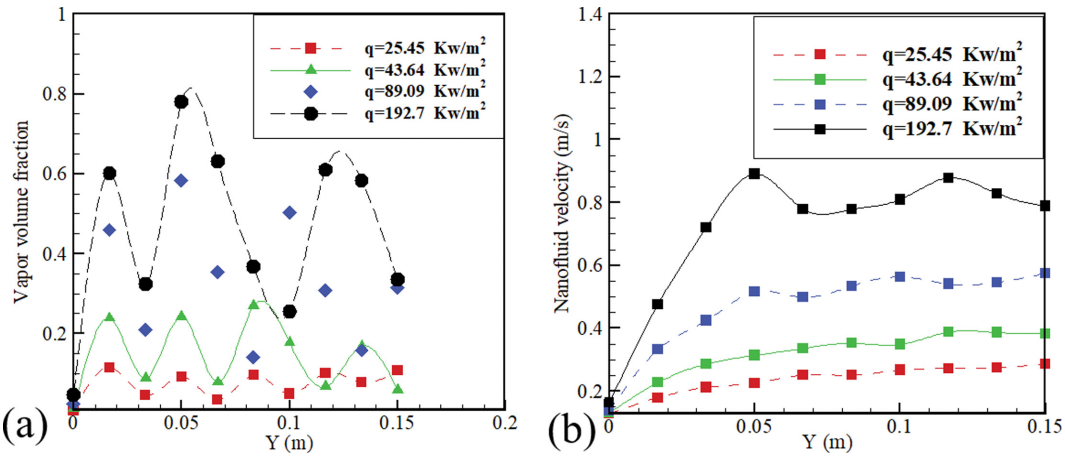

Fig. 12. Effects of heat flux on silica nanofluid (0.01% vol) pool boiling heat transfer characteristics (f_{vib}=10 Hz, and Y_{wall}=2 mm) at t=4 s (a) vapor volume fraction along the vertical distance and (b) nanofluid velocity along the vertical distance.

In Figs. 12(a) and 12(b) vapor volume fraction and nanofluid velocity along the vertical distance at t=4 s are shown for four different heat fluxes for silica nanofluid (0.01% vol). It is assumed that the heated surface is vibrating under the f_{vib}=10 Hz and Y_{wall}= 2 mm. According to Fig. 12(a), as the heat flux increases vapor volume fraction rises. This phenomenon is mainly due to the formation of bubbles during the nucleate boiling regime, and an increase in heat flux can make an improvement in the superheat temperature, which leads to a development in nucleation site density. As a consequence, agent bubbles become dominant on the heated surface and go up to the top of the boiling chamber due to the buoyancy effect. Fig. 12(b) indicates that the slope of nano-

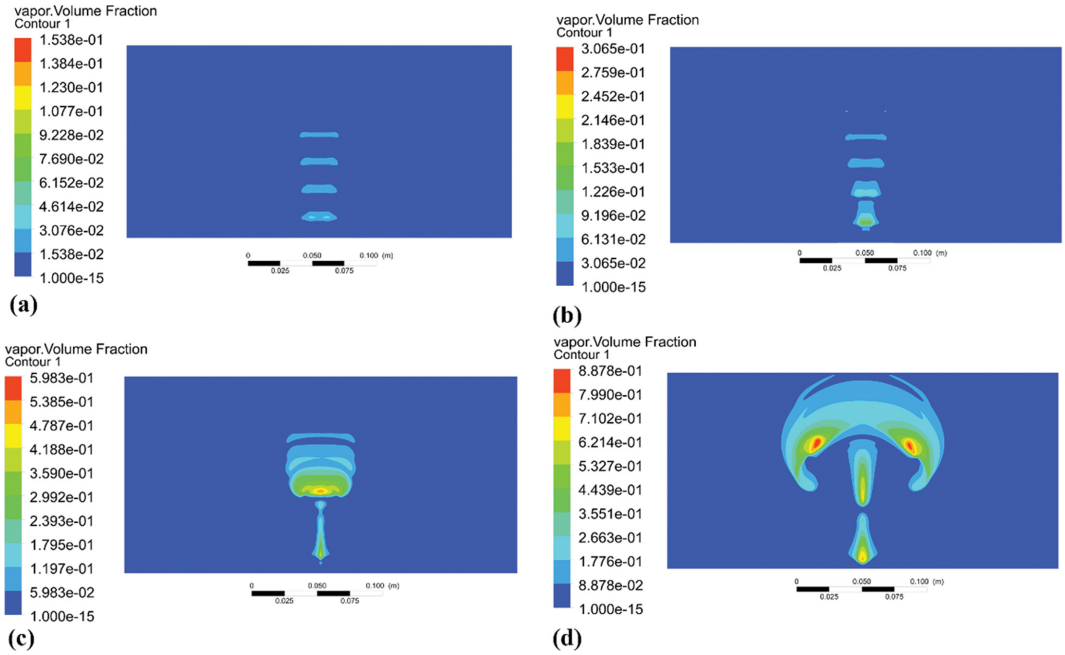

Fig. 13. Effect of mechanical vibration on vapor volume fraction for (a) q=25.45 kW/m^2, (b) q=43.64 kW/m^2, (c) q=89.09 kW/m^2, and (d) q= 192.7 kW/m^2 (t=0.7 s, f_{vib}=10 Hz, and Y_{wall}=2 mm).

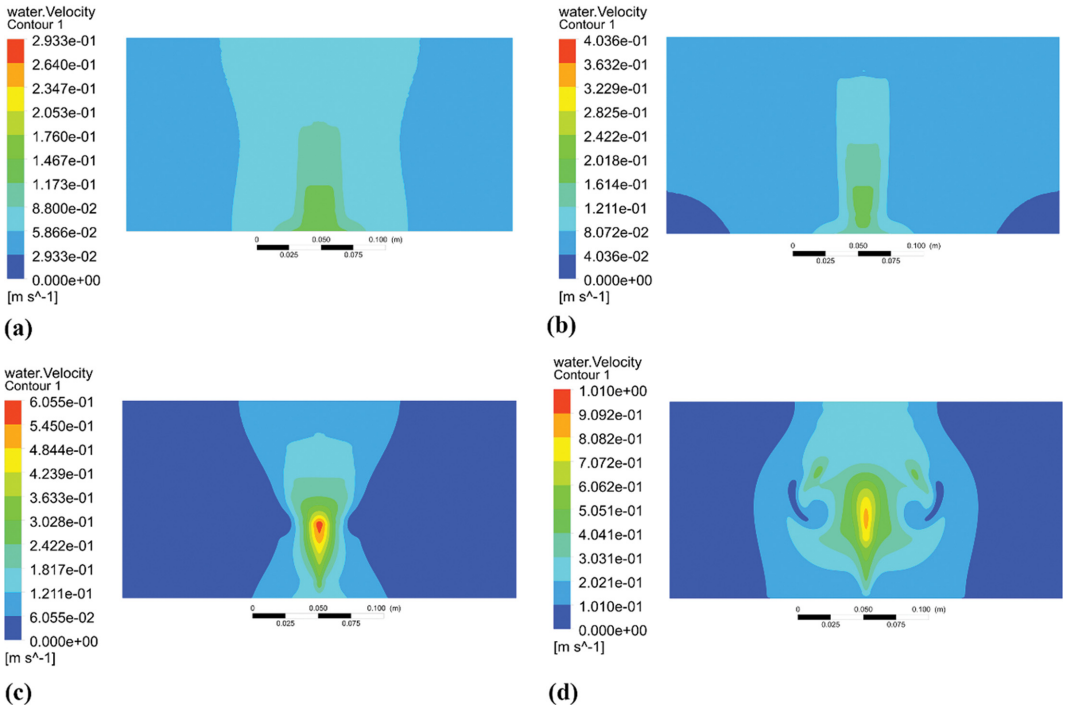

Fig. 14. Effect of mechanical vibration on nanofluid velocity for (a) q=25.45 kW/m^2, (b) q=43.64 kW/m^2, (c) q=89.09 kW/m^2, and (d) q= 192.7 kW/m^2 (t=0.7 s, f_{vib}=10 Hz, and Y_{wall}=2 mm).

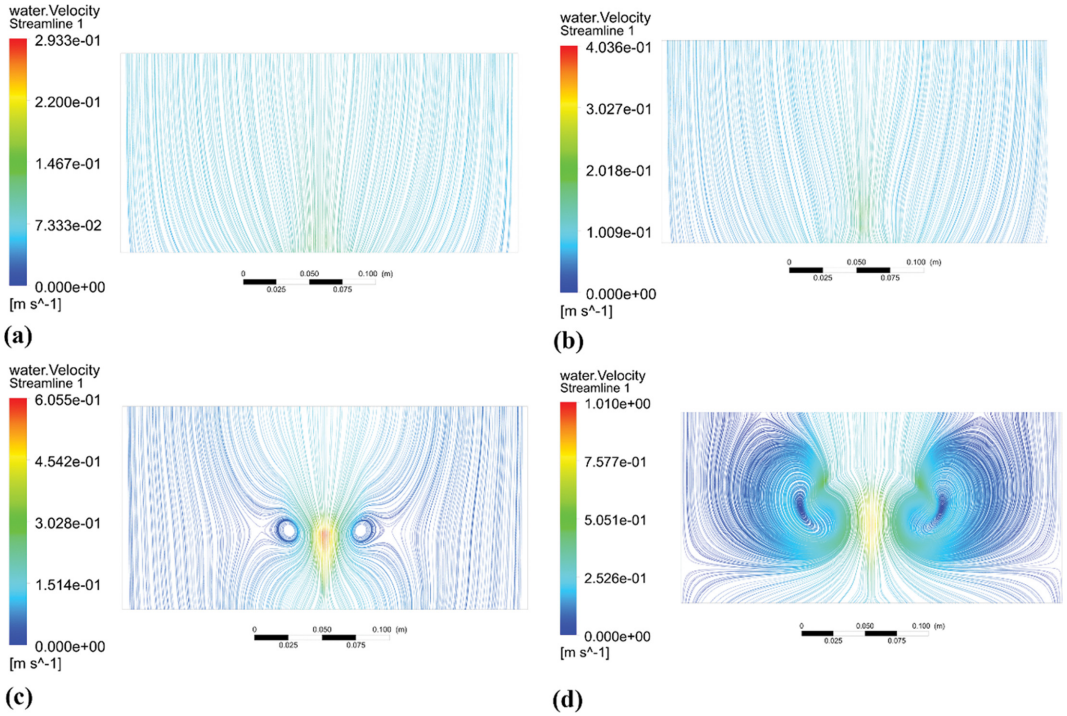

Fig. 15. Effect of mechanical vibration on streamlines for (a) q=25.45 kW/m^2, (b) q=43.64 kW/m^2, (c) q=89.09 kW/m^2, and (d) q=192.7 kW/m^2 (t=0.7 s, f_{vib}=10 Hz, and Y_{wall}=2 mm).

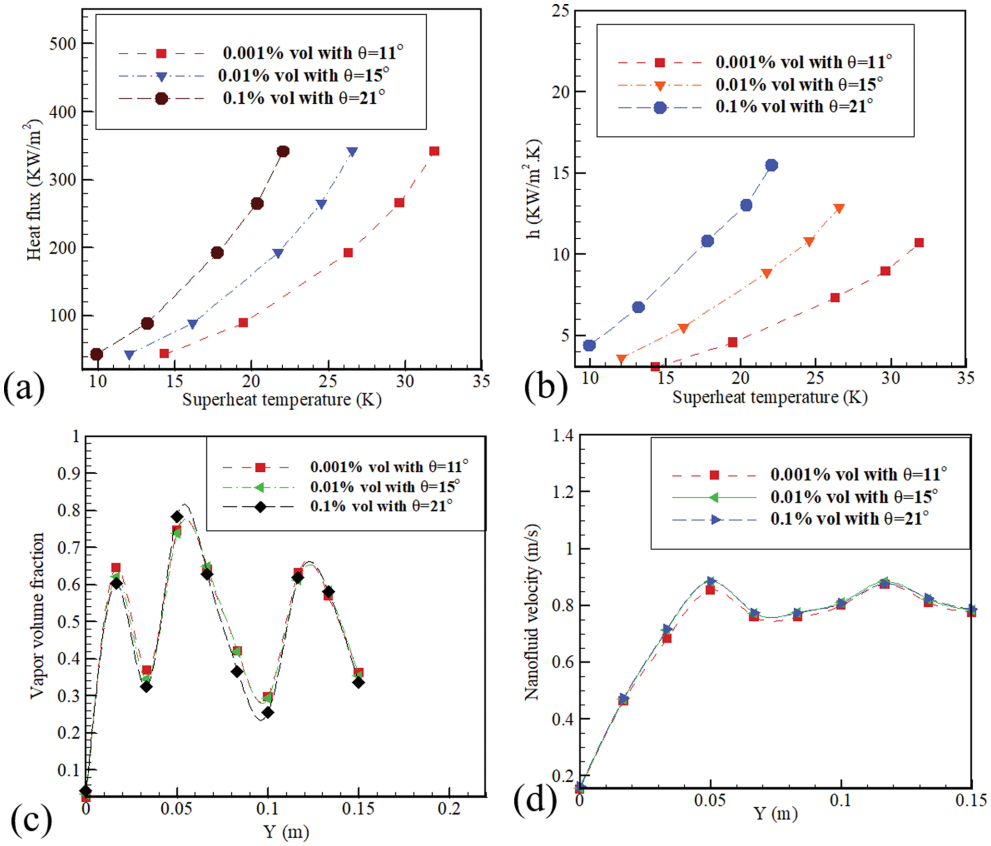

Fig. 16. Effect of silica nanofluid concentration on pool boiling heat transfer characteristics (f_{vib}=10 Hz, and Y_{wall}=2 mm) at t=4 s (a) boiling curve, (b) heat transfer coefficient, (c) vapor volume fraction along the vertical distance, and (d) nanofluid velocity along the vertical distance.

fluid velocity is so sharp near the heated surface, and as the heat flux increases nanofluid velocity enhances. This is due to the fact that by increasing the heat flux, thermal momentum transferred from the heated surface to the nanofluid leads to more agitation and turbulence in the fluid flow. Therefore, this momentum causes faster bubble detachment as well as a sudden increase in the nanofluid velocity near the heated surface.

In Figs. 13 to 15 contours of vapor volume fraction, nanofluid velocity and streamlines are compared for four different heat fluxes at t=0.7 s, f_{vib}=10 Hz, and Y_{wall}=2 mm for silica nanofluid (0.01% vol). According to these figures, as the heat flux increases mushroom shape of vapor volume fraction starts forming faster and eddies formed below the polar cap become larger.

4. The Effects of Nanofluid Concentration

Surface modifications achieved by adding nanoparticles into the base fluid, can affect nanofluid pool boiling performance. It should be taken into consideration that the material, size and concentration of nanoparticles affect bubble dynamic characteristics and the properties of corresponding nanofluid. Material and concentration would also manipulate the wettability of nanoparticle-deposited surface [33].

Fig. 16(a) shows the applied heat flux versus superheat temperature changes for different concentrations of silica nanofluid while the heated surface is vibrating at the frequency f_{vib}=10 Hz and the amplitude Y_{wall}=2 mm. According to Fig. 16(a), superheat temperature decreases when increasing the silica nanofluid concentration. This reduction is the main factor for the development of heat transfer coefficient. Fig. 16(b) compares the changes in the heat transfer coefficient for different concentrations of silica nanofluid while the heated surface is vibrating at the frequency f_{vib}=10 Hz and the amplitude Y_{wall}=2 mm. It illustrates that heat transfer coefficient is decreased by decreasing silica nanofluid concentration. This phenomenon was also addressed in previous experimental studies of Gerardi et al. [45] and Li et al. [33] conducted for different nanofluid concentrations on non-vibrating heated surface. The main reason that could lead to the reduction of heat transfer coefficient for nanofluid is the deposition of nanoparticles on the heating surface during the boiling process. This phenomenon builds up the porous nano-layer created due to the microlayer evaporation process on the heating surface. This can typically beef up surface wettability by reducing the contact angle between the liquid and surface. Furthermore, this nano-layer could act like a thermal resistance and exclude heat transfer rate from the surface to a liquid. Vapor volume fraction variation and nanofluid velocity along the vertical distance at t=4 s for different concentrations of silica nanofluid are shown in Figs. 16(c) and 16(d). In this case the heated surface is vibrating at the frequency f_{vib}=10 Hz and the amplitude Y_{wall}= 2 mm. It demonstrates that by increasing nanoparticle concentration, vapor volume fraction decreases. It will result from decreasing of wall temperature. In addition, nanofluid concentration does not affect nanofluid velocity in pool boiling heat transfer phenomenon.

5. Correlations for Pool Boiling Heat Transfer Parameters

This section presents the high-accuracy analytical correlations for computing silica nanofluid pool boiling heat transfer characteristics, such as heat transfer coefficient and nanofluid velocity. Superheat temperature, amplitude and frequency of vibration are utilized

Table 1. RMSE, R-Square and constant coefficients of correlations for Eq. (31) and Eq. (32)

Constants	C_1	C_2	C_3	C_4	C_5	C_6
h (Y_{wall}, T_{sup})	2.406	0.07168	−0.6513	0.07032	0.01761	0.1121
u_l (f_{vib}, y)	0.006708	0.01313	17.53	2.121e-05	−0.1086	−224.4
C_7	C_8	C_9	C_{10}	C_{11}	C_{12}	R-Square	RMSE
7.693e-05	−0.0007293	−0.002626	-	-	-	0.9996	0.1048
−0.01897	1.585	1206	0.1696	−11.63	−2220	0.9891	0.01781

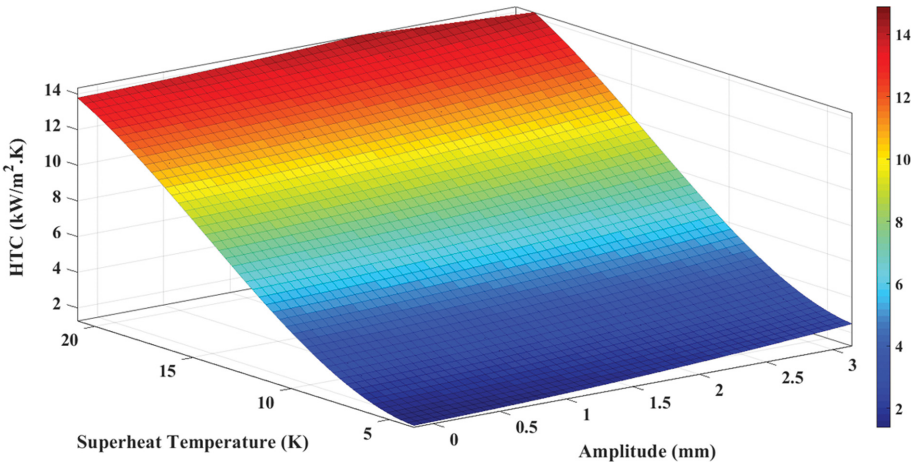

Fig. 17. Heat transfer coefficient based on superheat temperature and amplitude of vibration when f=10 Hz at t=4 s.

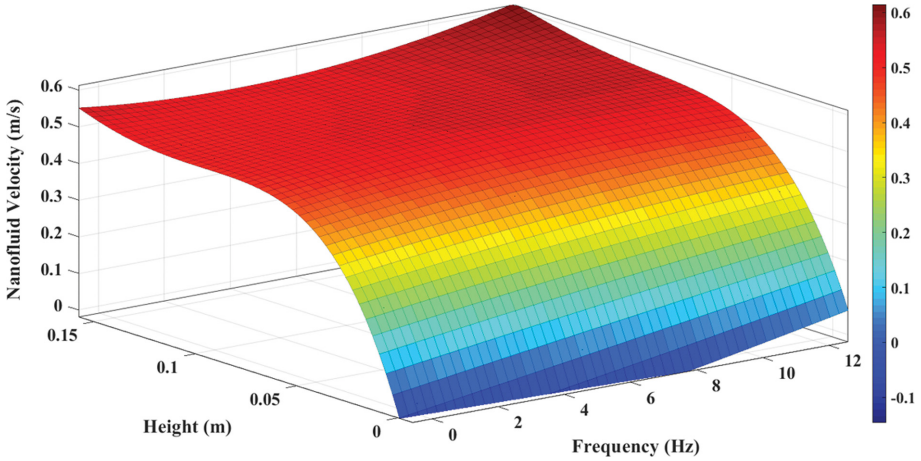

Fig. 18. Nanofluid velocity based on height of the boiling chamber and frequency of vibration (Y_{wall}=2 mm, and =89.09 kW/m^2) at t=4 s.

to introduce these correlations. Eq. (31) illustrates the correlation for the heat transfer coefficient based on the amplitude of vibration and superheat temperature. Furthermore, Eq. (32) is proposed to compute nanofluid velocity correlated with the frequency of vibration and height of the pool boiling chamber. Table 1 shows the coefficient constants, including RMSE and correlation coefficient in this study.

$$HTC(Y_{wall}, T_{sup}) = C_1 + C_2 \times Y_{wall} + C_3 \times T_{sup} + C_4 \times Y_{wall}^2 + C_5 \times Y_{wall} \times T_{sup} + C_6 \times T_{sup}^2 + C_7 \times Y_{wall}^2 \times T_{sup} + C_8 \times Y_{wall} \times T_{sup}^2 + C_9 \times T_{sup}^3 \quad (31)$$

$$u_l(f_{vib,y}) = C_1 + C_2 \times f_{vib} + C_3 \times y + C_4 \times f_{vib}^2 + C_5 \times f_{vib} \times y + C_6 \times y^2 + C_7 \times f_{vib}^2 \times y + C_8 \times f_{vib} \times y^2 + C_9 \times y^3 + C_{10} \times f_{vib}^2 \times y^2 + C_{11} \times f_{vib} \times y^3 + C_{12} \times y^4 \quad (32)$$

In Fig. 17, heat transfer coefficient is studied under the influence of amplitude of vibration and superheat temperature using Eq. (31) at t=4 s when f_{vib}=10 Hz. Amplitude of vibration ranges from 0 to 3 mm and superheat temperature goes up to 20 K. As can be seen, for different amplitude of vibration investigated in the present work, the maximum value of the heat transfer coefficient occurred at higher amplitude of vibration and the corresponding superheat temperature. This value is placed at the high-flux region of the pool boiling curve.

In Fig. 18, the impact of the frequency of vibration ranging from 0 to 12 Hz and the height of the pool boiling chamber on nanofluid velocity is investigated using Eq. (32) at t=4 s when Y_{wall}= 2 mm and q=89.09 kW/m^2. The maximum value of nanofluid velocity occurred at the top of the boiling chamber.

CONCLUSION

Numerical investigation of the effects of the heated surface vibration on nanofluid pool boiling heat transfer was addressed in the present work. Euler-Euler approach was used to simulate the interaction between vapor and nanofluid phases, based on transient simulation. The k-ε turbulence model was used for simulating the Reynolds stresses appeared in the averaged Navier Stokes equation. To account for the heat removal by vapor bubble nucleation and detachment from a solid surface, the RPI boiling method was adopted. Furthermore, a set of correlations for analyzing the heat transfer coefficient along with nanofluid velocity based on superheat temperature, amplitude and frequency of vibration are presented in this study. The main conclusions of the present work can be summarized as follows:

1) Implementation of surface vibration damped the eddies formed at heated surface and refined pool boiling heat transfer performance.

2) The augmentation effect of the heated surface vibration is most remarkable for moderately low heat fluxes for different amplitude and frequency of oscillations.

3) Increasing the amplitude of vibration can lead to an increase of up to 30.11% for q=10.91 kW/m^2 and 3.94% for q=265.5 kW/m^2, when Y_{wall}=3 mm and f_{vib}=10 Hz compared to non-vibrating surface. Moreover, augmentation of the frequency of vibration would give rise to an enhancement of up to 17.5% for q=10.91 kW/m^2 and 3.9% for q=341.8 kW/m^2 compared to non-vibrating surface, when Y_{wall}=2 mm and f_{vib}=10 Hz.

4) Amplitude of vibration improves the heat transfer rate a bit better than frequency of vibration.

5) Heat transfer coefficient increases with an increase in nanofluid concentration, and as the heat flux increases, the slope of boiling curve shifts towards lower superheat temperatures. As a consequence, increasing nanofluid concentration from 0.001% vol to 0.1% vol at q=341.8 kW/m^2, f=10 Hz and Y_{wall}=2 mm leads to an increment of up to 44.72% in heat transfer coefficient.

NOMENCLATURE

A_{tc} : fraction of heater area occupied by bubbles
a_{if} : interfacial area concentration [m^{-1}]
C_p : specific heat [J/kg·K]
y : height of the pool boiling chamber [m]
d_{bubble} : bubble diameter [m]
d_w : bubble departure diameter on the wall [m]
F_{lg} : action of interfacial forces from vapor on liquid [N]

F_{gl} : action of interfacial forces from liquid on vapor [N]
f : bubble departure frequency [Hz]
f_{vib} : heated wall vibration frequency [Hz]
Y_{wall} : vibration amplitude
α : volume fraction
S_i : additional source terms due to coalescence and break age [kg/m^3·s]
f_i : scalar fraction related to the number density of the discrete bubble classes
G : mass flux [kg/m^2·s]
Re : Reynolds number
Pr : Prandtl number
g : gravitational constant [m/s^2]
H : specific enthalpy [J/kg]
h : interfacial heat transfer coefficient [J/kg]
h_{fg} : specific latent heat of vaporization [J/kg]
k : conductivity [W/m^2·K]
m : mass [kg]
N_a : active nucleation site density [m^2]
P : pressure [N/m^2]
Q_c : heat transfer due to forced convective [W/m^2]
Q_e : heat transfer due to forced evaporation [W/m^2]
Q_{tc} : heat transfer due to transient conduction [W/m^2]
T : temperature [K]
T_{sup} : wall superheat temperature [K]=$T_w - T_{sat}$
T_w : wall temperature [K]
ΔT : difference in temperature [K]
t : time [s]
u : velocity [m/s]
y^+ : non-dimensional distance to the wall

Greek Symbols

μ : viscosity [Pa·s]
ρ : density [kg/m^3]
σ : surface tension [N/m]
Γ_{lg} : interfacial mass transfer from vapor to liquid [kg/m^3·s]
Γ_{gl} : interfacial mass transfer from liquid to vapor [kg/m^3·s]
φ : volume fraction [%]

Subscript

g : vapor
l : liquid
W : wall
θ : contact angle [°]
eff : effective

REFERENCES

1. B. Sutharshan, M. Mutyala, R. Vijuk and A. Mishra, *Energy Procedia*, **7**, 293 (2011).
2. E. Çiftçi and A. Sözen, *Heat Transf. Res.*, **51**, 10431059 (2020).
3. H. Alimoradi, M. Shams, N. Ashgriz and A. Bozorgnezhad, *Case Stud. Therm. Eng.*, **24**, 100829 (2020).
4. M. H. Zolfagharnasab, M. Salimi, H. Zolfagharnasab, H. Alimoradi, M. Shams and C. Aghanajafi, *Powder Technol.*, **380**, 1 (2021).
5. J. Ham and H. Cho, *Appl. Therm. Eng.*, **108**, 158 (2016).
6. H. Alimoradi, M. Shams and Z. Valizadeh, *Modares Mech. Eng.*, **16**(12), 545 (2017).
7. A. Bozorgnezhad, M. Shams, H. Kanani and M. Hasheminasab, *J. Dispers. Sci. Technol.*, **36**(8), 1190 (2015).
8. H. Alimoradi and M. Shams, *Modares Mech. Eng.*, **19**(7), 1613 (2019).
9. M. Roodbari, H. Alimoradi, M. Shams and C. Aghanajafi, *J. Therm. Anal. Calorim.*, 1 (2021).
10. E. Çiftçi and A. Sözen, *Int. J. Numer. Methods Heat Fluid Flow.*, **31**, 2652 (2020).
11. S. Etedali, M. Afrand and A. Abdollahi, *Int. J. Therm. Sci.*, **145**, 105977 (2019).
12. V. Sajith, M. R. Madhusoodanan and C. B. Sobhan, *ASME 2008*, 555561 (2008).
13. M. Hasheminasab, A. Bozorgnezhad, M. Shams, G. Ahmadi and H. Kanani, in: ASME 2014 12th Int. Conf. Nanochannels, Microchannels Minichannels, ICNMM2014-21586, V001T07A002, Chicago, Illinois (2014).
14. A. Bozorgnezhad, M. Shams, G. Ahmadi, H. Kanani and M. Hasheminasab, in: ASME/JSME/KSME 2015 Jt. Fluids Eng. Conf., AJKFluids2015-22299, V001T22A004, Seoul, South Korea (2015).
15. A. Bozorgnezhad, M. Shams, H. Kanani, M. Hasheminasab and G. Ahmadi, *Int. J. Hydrogen Energy*, **41**(42), 19164 (2016).
16. M. Ashrafi, M. Shams, A. Bozorgnezhad and G. Ahmadi, *Heat Mass Transf.*, **52**(12), 2671 (2016).
17. H. Atashi, A. Alaei, M. H. Kafshgari, R. Aeinehvand and S. K. Rahimi, *Exp. Heat Transf.*, **27**(5), 428 (2014).
18. J. H. Jeong and Y. C. Kwon, *Heat Mass Transf. und Stoffuebertragung*, **42**(12), 1155 (2006)
19. N. Unno, K. Yuki, J. Taniguchi and S. Satake, *Int. J. Heat Mass Transf.*, **153**, 119588 (2020).
20. A. Sathyabhama and S. P. Prashanth, *Heat Transf. - Asian Res.*, **46**, 4960 (2015).
21. H. Y. Kim, Y. G. Kim and B. H. Kang, *Int. J. Heat Mass Transf.*, **47**(12-13), 2831 (2004).
22. S. Alangar, *Heat Mass Transf. und Stoffuebertragung*, **53**(1), 73 (2017).
23. H. Alimoradi and M. Shams, *Appl. Therm. Eng.*, **111**, 1039 (2017).
24. S. N. Shoghl, M. Bahrami and M. K. Moraveji, *Int. Commun. Heat Mass Transf.*, **58**, 12 (2014).
25. Z. Valizadeh and M. Shams, *Heat Mass Transf. und Stoffuebertragung*, **52**(8), 1501 (2016).
26. M. S. Kamel, M. S. Al-agha, F. Lezsovits and O. Mahian, *J. Therm. Anal. Calorim.*, **142**, 493505 (2019).
27. S. M. A. N. R. Abadi, A. Ahmadpour and J. P. Meyer, *Int. J. Multiph. Flow*, **118**, 97 (2019).
28. H. Shokouhmand and S. M. A. N. R. Abadi, *Heat Mass Transf. und Stoffuebertragung*, **46**(8-9), 891 (2010).
29. H. Shokouhmand, S. M. A. Noori Rahim Abadi and A. Jafari, *Int. J. Mech. Mater. Des.*, **7**, 313 (2011).
30. J. Vadasz, J. Meyer and S. Govender, *Transp. Porous Media*, **103**, 279294 (2014).
31. X. Li, K. Li, J. Tu and J. Buongiorno, *Int. J. Heat Mass Transf.*, **69**, 443 (2014).
32. X. Li, Y. Yuan and J. Tu, *Int. J. Heat Mass Transf.*, **91**, 467 (2015).
33. X. Li, Y. Yuan and J. Tu, *Int. J. Therm. Sci.*, **98**, 42 (2015).

34. M. Mohammadpourfard, H. Aminfar and M. Sahraro, *Heat Mass Transf. und Stoffuebertragung*, **50**(8), 1167 (2014).
35. R. L. Hamilton and O. K. Crosser, *Ind. Eng. Chem. Fundam.*, **1**, 187 (1962).
36. H. C. Brinkman, *J. Chem. Phys.*, **20**(4), 571 (1952).
37. M. Ishii and N. Zuber, *AIChE J.*, **25**(5), 843 (1979).
38. W. E. Ranz and W. R. Marshall, *Chem. Eng. Progress*, **48**, 141146 (1952).
39. M. Lopez de Bertodano, R. T. Lahey and O. C. Jones, *Nucl. Eng. Des.*, **146**, 4352 (1994).
40. N. Kurul and M. Z. Podowski, *Proceedings of 27th national heat transfer conference at minnieapolis*, MN, USA, 2831 (1991).
41. N. Kurul and M. Z. Podowski, *Proceedings of the 9th international heat transfer conference at Jerusalem*, 2, 2126 (1990).
42. H. Salehi and F. Hormozi, *Heat Mass Transf.*, **54**, 773784 (2017).
43. E. Krepper, B. Končar and Y. Egorov, *Nucl. Eng. Des.*, **237**(7), 716 (2007).
44. V. I. Tolubinsky and D. M. Kostanchuk, Vapour bubbles growth rate and heat transfer intensity at subcooled water boiling, in *International Heat Transfer Conference* ***4***, 23 (1970).
45. C. Gerardi, J. Buongiorno, L. Hu and T. Mckrell, *Nanoscale Res. Lett.*, **6**, 232 (2011).
46. R. Cole, *AIChE J.*, **6**(4), 533 (1960).
47. A. Akbari, S. A. Alavi Fazel, S. Maghsoodi and A. S. Kootenaei, *J. Therm. Anal. Calorim.*, **135(**1), 697 (2019).
48. H. Aminfar, M. Mohammadpourfard and M. Sahraro, *Comput. Fluids*, **66**, 29 (2012).